ELSEVIER

Journal of Nuclear Materials 276 (2000) 278–282

journal of nuclear materials

www.elsevier.nl/locate/jnucmat

A new procedure of X-ray line profile analysis applied to study the dislocation structure and subgrain size-distributions in fatigued MANET steel

T. Ungár[a,*], M. Victoria[b], P. Marmy[b], P. Hanák[a], G. Szenes[a]

[a] *Department of General Physics, Eötvös University Budapest, H-1518, P.O. Box 32, H-1518 Budapest VIII, Hungary*
[b] *Ecole Polytechnique Federale de Lausanne/Centre de Reserches en Physique des Plasmas, Ass. EURATOM-Conf. Suisse, CH-5232 Villingen-PSI, Hungary*

Abstract

A new procedure of X-ray line profile analysis based on the dislocation model of strain anisotropy has been applied. The dislocation densities and the subgrain size-distributions in a MANET steel are investigated in the normal condition and after cyclic deformation at room temperature and 250°C. It has been found that the average dislocation density in the normal condition is rather high and does not change much after fatigue at room temperature. After fatigue at 250°C, however, the dislocation density was found to increase considerably, probably due to the strong temperature dependence of the mobility of dislocation in a martensitic steel. Even though the subgrain size-distribution was found not to change much on fatigue at room temperature, it widened however after fatigue at 250°C.

1. Introduction

In the European Fusion Materials Technology Programme the 1.4914 ferritic/martensitic steel was originally one of the candidates for first wall materials, and it was on its basis that the low activation compositions studied at present were developed. Transmission electron microscopy (TEM) and low cycle fatigue (LCF) investigations have shown that subsize and bulk specimens reveal similar results concerning the microstructure and mechanical properties [1,2]. The results obtained on the subsize specimens also compare well with other investigations on bulk material [3]. In a previous study it was found that the strength of the tempered martensite is caused by the carbide precipitates and by the lath structure which is strengthened by a high density of dislocation [1]. TEM observations have shown that after tensile deformation or LCF a well-developed dislocation cell structure is formed leaving very little of the original dislocation density in the martensite. It was concluded further that the strength in this state is caused by carbides and solute elements in the martensite [1].

In the present investigation, the same type of subsize specimens as investigated in reference [1] are revisited by a new procedure of X-ray line profile analysis [4] in order to determine the dislocation densities, the subgrain size-distribution in the tempered state and after LCF of the material.

2. Experimental

2.1. Specimens

The specimens were prepared from the European MANET cast of 1.4914 steel. After homogenisation at 950°C the material was austenitised at 1075°C and tempered at 750°C, this state will be denoted as normal condition. After sample preparation stress relief treatment at 650°C was applied. The LCF tests were carried out on tubular specimens of wall thickness 0.34 mm in an electromechanical, computer controlled, closed-loop

* Corresponding author. Tel.: +36-1 266 7927; fax: +36-1 266 7927.
E-mail address: ungar@ludens.elte.hu (T. Ungár)

0022-3115/00/$ - see front matter
PII: S0022-3115(99)00223-8

testing machine. More details about specimen preparation can be found in [1]. For the X-ray diffraction measurements 1.5×1.5 mm^2 samples were prepared by spark erosion and chemically etched to remove surface damage. In the present work MANET steel in the following three states was investigated: (1) in the normal condition, before the fatigue tests, (2) after fatigue test at room temperature (RT) at a total strain amplitude of $\Delta\varepsilon_t = 0.75\%$ and a plastic strain amplitude of $\Delta\varepsilon_{pl} = 0.325\%$ for 15,500 cycles and 3) after fatigue test at 250°C at a total strain amplitude of $\Delta\varepsilon_t = 0.6\%$ and a plastic strain amplitude of $\Delta\varepsilon_{pl} = 0.202\%$ for 22,000 cycles.

2.2. X-ray diffraction technique

The diffraction profiles were measured by a special double crystal diffractometer with negligible instrumental broadening [4,5]. A fine focus rotating cobalt anode, Nonius FR 591, was operated as a line focus at 35 kV and 50 mA. The symmetrical 220 reflection of a Ge monochromator was used in order to have wavelength compensation in the lower angle region. The $K\alpha_2$ component of the Co radiation was eliminated by a 0.2 mm slit between the source and the Ge crystal. By curving the Ge crystal sagittally in the plane perpendicular to the plane-of-incidence the brilliance of the diffractometer was increased by a factor of 5. The profiles were registered by a linear position sensitive gas flow detector, OED 50 Braun, Munich. The instrumental line broadening was kept below 5% of the physical broadening by setting the distance between specimen and detector to 0.5 m. For avoiding air scattering and absorption this distance was overbridged by an evacuated tube closed by mylar windows.

2.3. Evaluation of diffraction profiles

The FWHM and the integral breadths of the diffraction profiles are evaluated by the *modified* Williamson–Hall plot [4]

$$\Delta K \cong 0.9/D + (\pi M^2 b^2/2)^{1/2}\rho^{1/2}KC^{1/2} + \mathrm{O}(K^2C), \qquad (1)$$

where $K = 2\sin\theta/\lambda$, $\Delta K = 2\cos\theta(\Delta\theta)/\lambda$, θ and λ are the diffraction angle and the wavelength of X-rays, and D, ρ and b are the average particle size, the average dislocation density and the Burgers vector of dislocations, respectively. M is a constant depending on the effective outer cut-off radius of dislocations. M can only be obtained from the tails of the profiles [6], therefore, it will be determined from the Fourier coefficients as shown below. C is the dislocation contrast factor depending on the relative orientations between the Burgers and line vectors of dislocations and the diffraction vector [4].

In a recent investigation it was shown that the average dislocation contrast factors can be given as [7]

$$\overline{C} = \overline{C}_{h00}(1 - qH^2), \qquad (2)$$

where $\overline{C}_{h00}$ is the average dislocation contrast factor for the *h00* reflections (in cubic crystals), q is a parameter depending on the elastic constants of the crystal and the character of dislocations in the crystal [8] and

$$H^2 = \frac{h^2k^2 + h^2l^2 + k^2l^2}{(h^2 + k^2 + l^2)^2}. \qquad (3)$$

Inserting Eqs. (2) and (3) into Eq. (1) yields

$$\Delta K \cong \alpha + \beta K^2\overline{C}_{h00}(1 - qH^2), \qquad (4)$$

where $\alpha = (0.9/D)^2$ and $\beta = \pi M^2 b^2\rho/2$. The values of q and α were obtained by the method of least squares from Eq. (4). The values of $\overline{C}_{h00}$ can be obtained from the tables in [8], in the case of iron $\overline{C}_{h00} = 0.285$. On the basis of Fig. 2 in [8] the experimental values of q provide information about the screw, edge or mixed character of dislocations.

The dislocation density can be obtained from the *modified* Warren–Averbach method [4]

$$\ln A(L) \cong \ln A^s(L) - \rho BL^2 \ln(R_e/L)(K^2\bar{C}) + \mathrm{O}(K^4C^2), \qquad (5)$$

where $A(L)$ is the real part of the Fourier coefficients, A^s is the size Fourier coefficient as defined by Warren [9], $B = \pi b^2/2$, R_e is the effective outer cut-off radius of dislocations and O stands for higher order terms in $K^2\overline{C}$. L is the Fourier length defined as [9]: $L = na_3$, where $a_3 = \lambda/2(\sin\theta_2 - \sin\theta_1)$, n are integers starting from zero and $(\theta_2 - \theta_1)$ is the angular range of the measured diffraction profile. The average particle size, obtained from the size Fourier coefficients A^s is denoted by L_0.

2.4. Size distribution

According to Eqs. (4) and (5) three different particle sizes can be obtained: (i) D from the FWHM, (ii) d from the integral breadths and (iii) L_0 from the Fourier coefficients. These three gauges sample the largest, the medium and the smallest characteristic lengths in the specimen since they are related to the central part, the integral and the outermost tails of the profiles, respectively. At the same time, these three gauges are rather stable and only restrictedly vulnerable to experimental errors or fluctuations [10]. A simple numerical procedure has been worked out recently to relate the experimentally determined D, d and L_0 values to the parameters of a size distribution function, $f(x)$, especially for a log-normal size distribution [10]

$$f(x) = \frac{1}{\sqrt{2\pi}\sigma}\frac{1}{x}\exp\left\{-\frac{(\ln x - m)^2}{2\sigma^2}\right\}, \quad (6)$$

where x is the average particle size in the direction of the diffraction vector, σ the width of size distribution and m the momentum of the probability density function. (In the literature of line profile analysis the average particle size in the direction of the diffraction vector is called average 'column length' [9]). We denote the size function of a particle (in the direction of the diffraction vector) by $V(x)$: $V(x) = 1$ inside and $V(x) = 0$ outside the particle. If the particle is distortion free the scattered intensity is the square of the Fourier transform of $V(x)$ [11]

$$I(K) = \left(\frac{\sin Kx_0}{Kx_0}\right)^2, \quad (7)$$

where x_0 is the average particle size (or column length). Assuming that the particles in the specimen have the size distribution $f(x)$ the scattered intensity is

$$I^s(K) = \int_0^\infty f(x)\left(\frac{\sin Kx}{Kx}\right)^2 dx, \quad (8)$$

where the superscript s refers to 'size'. The experimental D, d and L_0 values are matched to the numerically calculated $I^s(K)$ function by the method of least squares. As the result of this numerical calculation the two parameters, σ and m corresponding to the log-normal size distribution are obtained.

3. Results and discussion

The FWHM corresponding to the three different states are shown in the *classical* Williamson–Hall plot [12] in Fig. 1. The deviations of the data from smooth curves exceed the experimental errors indicating a strong strain anisotropy. The same values are plotted according to Eq. (1) in Fig. 2. For the experimental value $q_{exp} = 2.6 \pm 0.1$ (see in Eqs. (2) and (4)) was obtained. In a recent work the values $\overline{C}_{h00}$ and q were evaluated for dislocations with Burgers vectors $a/2\ \langle 1\,1\,0\rangle$ and $a/2\langle 1\,1\,1\rangle$ [8] where it was shown that for iron $\overline{C}_{h00} = 0.285$. From the numerically calculated q values (see Fig. 2(b) in [8]) it follows that $q_{exp} = 2.6$ corresponds to dislocations with more screw than edge character in agreement with TEM observations in bcc iron [13] and ferritic–martensitic steels [14].

The Fourier coefficients corresponding to the 'normal condition' specimen are shown in the *modified* Warren–Averbach plot according to Eq. (5) in Fig. 3. The size

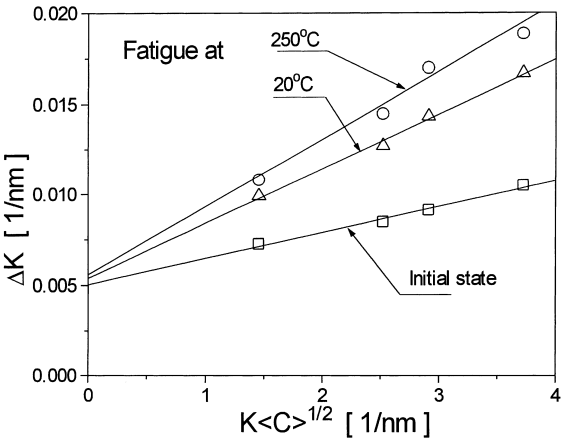

Fig. 2. The *modified* Williamson–Hall plot of the FWHM corresponding to the three different states of the MANET steel according to Eq. (1). (We note that $\langle C\rangle$ means the same average as the dash in Eq. (2).) The Miller indices are indicated in the figure. The symbols correspond to those of Fig. 1

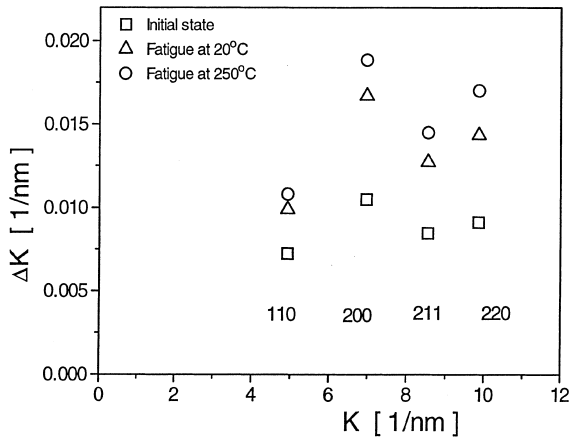

Fig. 1. The *classical* Williamson–Hall plot of the FWHM corresponding to the three different states of the MANET steel. The Miller indices are indicated in the figure.

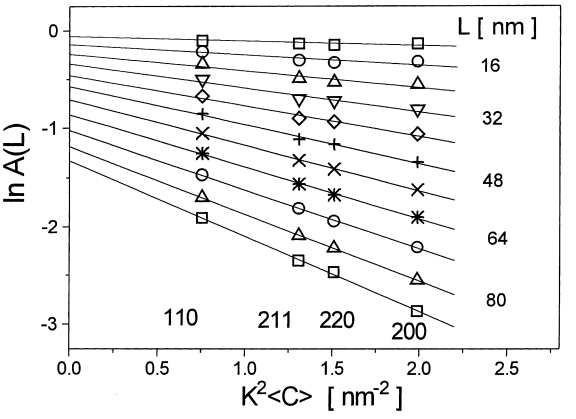

Fig. 3. The *modified* Warren–Averbach plot of the Fourier coefficients according to Eq. (5) of the normal condition specimen. The Miller indices are indicated in the figure. In a few cases the Fourier lengths L are shown at the lines.

Fourier coefficients $A^s(L)$ and the dislocation densities and effective outer cut-off radii, ρ and R_e, were obtained from the intercepts at $L=0$ and the initial slopes of the quadratic curves fitted to the data points by the method of least squares. The average particle size L_0 was obtained from $A^s(L)$ by the standard method described by Warren [9]. Here we note that due to the dislocation model of strain anisotropy formulated mathematically in Eqs. (1) and (5) as the *modified* Williamson–Hall and Warren–Averbach methods, respectively, not only the harmonics corresponding to one set of lattice planes, but all Bragg reflections can be used in line profile analysis, as shown in Figs. 2 and 3. From the FWHM, the integral breadths and the Fourier coefficients for three different particle size values, D, d and L_0, were obtained which were used to obtain the parameters σ and m of the log-normal size distribution functions. Fig. 4(a) shows the log-normal subgrain size-distribution function $f(x)$ of the specimen in normal condition and after fatigue at 250°C. The size distribution of the surface volume fraction $x^2f(x)$ is plotted in Fig. 4(b). It can be seen that the size distribution has become considerably wider after fatigue at 250°C in agreement with TEM observations (see the TEM micrographs in Fig. 2 in Ref. [1]) as pronounced strongly in Fig. 4(b). The values of the three different particle sizes, D, d and L_0, the dislocation densities and effective outer cut-off radii, ρ and R_e, and the parameters of the log-normal size distribution functions, σ and m, for the three different specimen are listed in Table 1.

The results of the X-ray diffraction experiments show that the dislocation density in the normal condition is relatively high: $\rho=1.5\times10^{14}$ m^{-2}. This is in good agreement with TEM observations, which also revealed a high dislocation density in the martensitic lath structure [1]. After fatigue at RT the dislocation density increases by about a factor of two and the sugrain size-distribution does not change considerably. In the martensitic laths the dislocations are distributed more or less uniformly. During fatigue the martensitic laths are gradually replaced by dislocation cells. The larger average dislocation density means that the dislocation content of the cell walls becomes rather high after fatigue at RT. After fatigue at 250°C, on the other hand, the dislocation density increases by about a factor of 8 and the size-distribution of subgrains becomes definitely wider. This is in good correlation with TEM observations showing the strong fragmentation of the initially long martensitic laths [1]. The large increase of the dislocation density after fatigue at 250°C is most probably related to the considerable enhancement of dislocation mobility at higher temperatures in bcc steels [15], which

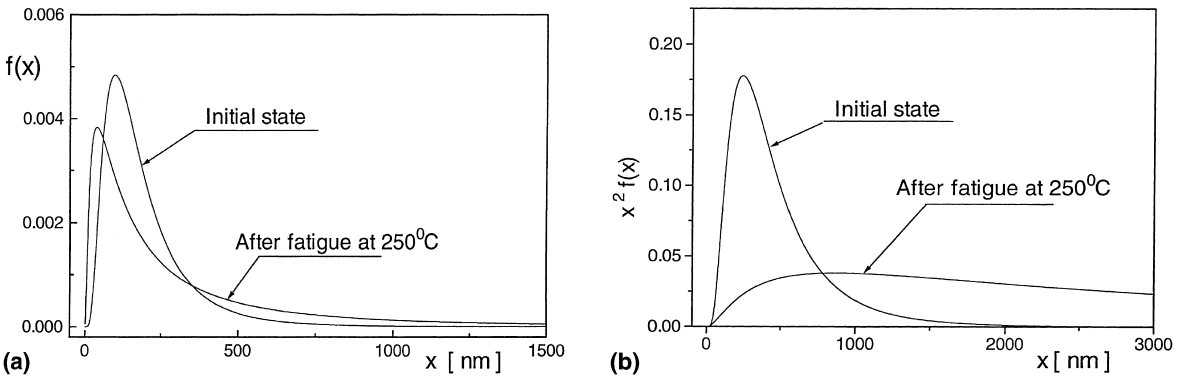

Fig. 4. The log-normal size distribution functions $f(x)$ (a) and the surface distribution function $x^2f(x)$, (b) of the dislocation cells or subgrains in the normal condition and after fatigue at 250°C. The functions were calculated according to Eq. (6) with the parameters in Table 1.

Table 1
The particle size values, D, d and L_0, the dislocation densities and arrangement parameters, ρ and M and the parameters of the log-normal size distribution functions, σ and m for the three different specimens

Specimen	D (nm)	d (nm)	L_0 (nm)	ρ (10^{14} m^{-2})	M	σ	m (nm)
Normal condition	184	130	112	1.5	1.9	0.67	154
Fatigue at RT	171	122	69	3.8	3.0	0.78	143
Fatigue at 250°C	224	110	62	12	2.0	1.25	182

promotes the formation of dislocation cells and the accumulation of dislocations in cell walls.

4. Conclusion

1. The dislocation model of the mean-square-strain enables the rationalisation of strain anisotropy.
2. The *modified* Williamson–Hall plot and Warren–Averbach procedures enable to determine correctly the strain and size contribution to X-ray line broadening.
3. The density and the arrangement parameter of dislocations, ρ and M can be obtained from the Fourier coefficients using the *modified* Warren–Averbach procedure on all available profiles.
4. From the three most stable size parameters of the line profiles the size distribution function of subgrains and/or dislocation cells can be obtained.
5. In a MANET steel it has been shown that:
   (a) the dislocation density in the initial-state or normal-condition is relatively high, in good agreement with TEM observations,
   (b) after fatigue at RT the dislocation density increases only by about a factor of two,
   (c) however, after fatigue at 250°C the dislocation density increases by about a factor of eight
   (d) the subgrain size-distribution does not change considerably after fatigue at RT, however, becomes considerably wider after fatigue at 250°C, in good correlation with TEM observations,
   (e) the large increase of the dislocation density after fatigue at 250°C is most probably related to the considerable enhancement of dislocation mobility at higher temperatures in bcc steels.

Acknowledgements

T.U. and G.Sz. are grateful for the support of the Hungarian National Science Foundation, OTKA, Grant No. T 022968 and T 022976 and the Hungarian Government Fund FKFP 0116/1997.

References

[1] P. Marmy, R. Yuzhen, M. Victoria, J. Nucl. Mater. 179 (1991) 697.
[2] P. Marmy, M. Victoria, in: D.G. Brandon, R. Chaim, R.A. Rosen (Eds.), Proceedings of the International Conference on Strength of Metals and Alloys, ICSMA 9 Haifa, vol. 2, 1991, p. 841.
[3] E.A. Little, L.P. Stoter, in: H.R. Brager, J.S. Perrin (Eds.), ASTM STP 782, 1982, p. 207.
[4] T. Ungár, A. Borbély, Appl. Phys. Lett. 69 (1996) 3173.
[5] M. Wilkens, H. Eckert, Z. Naturforsch. 19a (1964) 459.
[6] M. Wilkens, Phys. Stat. Sol. (a) 2 (1970) 359.
[7] T. Ungár, G. Tichy, Phys. Stat. Sol. (a) 171 (1999) 425.
[8] T. Ungár, I. Dragomir, Á. Révész, A. Borbély, J. Appl. Crystallogr. 32 (1999) 992.
[9] B.E. Warren, Progr. Metal Phys. 8 (1959) 147.
[10] T. Ungár, A. Borbély, G.R. Goren-Muginstein, S. Berger, A.R. Rosen, Nanostructured Mater. 11 (1999) 103.
[11] A. Guinier, X-ray Diffraction, Freeman, San Francisco, CA, 1963.
[12] G.K. Williamson, W.H. Hall, Acta Metall. 1 (1953) 22.
[13] B. Sestak, A. Seeger, Z. Metallkde. 69 (1978) 195, 355, 455.
[14] R. Schäublin, P. Spätig, M. Victoria, J. Nucl. Mater. 258–263 (1998) 1178.
[15] R.W.K. Honeycomb, in: The Plastic Deformation of Metals, Edward Arnold, London, 1968, p. 238.